A Miniature Water Surface Jumping Robot

Fei Jiang, Jianguo Zhao, Arun K. Kota, Ning Xi, Matt W. Mutka, and Li Xiao

***Abstract*—Many small insects such as water striders can leap from water surface. Inspired by their jumping capability, we present the design of a novel, miniature, water surface jumping robot in this paper. Jumping from water surface is more challenging than jumping from ground due to the liquid water surface. We address this problem by using carbon fiber strip to store energy, two wings to flap the water surface, a hollow body to initially support the robot, and an intermittent gear train to charge and release energy. With such a design, the final robot weighs around 12.5 g and has a maximum size of 10 cm. Experimental results show that the robot can jump up to 9.5 cm in height, which is close to the predicted results from a dynamic model developed by us to capture the hydrodynamic behaviors of the robot during the whole jumping process. The research presented in this paper offers a new design of tiny robots for mimicking the water-jumping capability of aquatic insects. The robot, if equipped with sensors, can be employed for aquatic environmental monitoring of water quality.**

***Index Terms*—Kinematics, mechanism design of mobile robots, biologically inspired robotics.**

I. Introduction

BEING able to monitor water quality is critical for people's health. Sensor networks with mobile aquatic sensors have been proposed as an effective way to dynamically monitor water quality (e.g., pollution levels or salinity). However, existing aquatic sensors (e.g., robotic boats) have a limited wireless communication range on water surface, thereby requiring a large number of sensors to monitor a specific area to ensure the network's connectivity. Mobile sensors with jumping capability can significantly extend the communication range by more than six times [1]. Therefore, a much smaller number of water surface jumping sensors is sufficient to cover the same area.

For the last decade, numerous robots have been developed to effectively jump from solid ground. Jianguo Zhao *et al.* [2], [3] designed a miniature robot that can wheel on flat ground, and self-right to leap over obstacles. Kovač *et al.* [4] designed a 7 grams robot which could jump over obstacles more than 27 times its own size. They also updated their jumping robot with self-recovery and steering capabilities [5]. Besides these two robots, many other ground jumping robots have been recently developed [6]–[11].

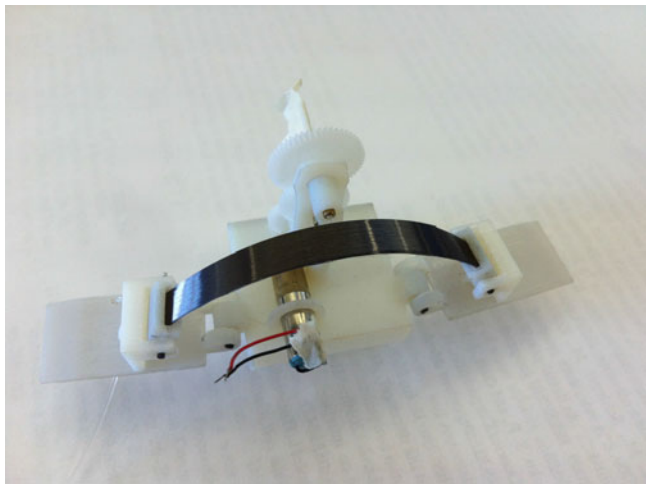

Fig. 1. Prototype for the water jumping robot.

Unlike jumping from solid ground, the yielding properties of water pose a challenge in developing robots that can jump from the water surface with similar effectiveness. Nevertheless, numerous small and high density creatures leverage water properties such as surface tension and added mass as well as hydrophobic appendages to elegantly take off from water surface [12]. For example, water striders [13], [14] can walk and jump on water surface easily with their hydrophobic legs. Globular springtail is able to jump by rapidly extending its furcula, which is normally folded under its abdomen [15], [16].

The superior speed and agility of these creatures have inspired researchers to design novel biologically inspired water jumping robots. Shin *et al.* [17] designed a miniature water jumping robot using a latch mechanism driven by shape memory alloy. Koh *et al.* [18] built a 68-milligram jumping robotic insect that was driven by the dominant surface tension. The power for jumping came from a torque reversal catapult mechanism, inspired by a flea's jumping legs. Jie Zhao *et al.* [19] designed a water jumping robot by mimicking the rowing locomotion of water striders. The robot weighed 10 grams and utilized super hydrophobic nickel foam sheets as supporting legs and a spring-based actuating mechanism. The same group recently improved their robot [20]

Manuscript received September 10, 2016; accepted January 13, 2017. Date of publication February 1, 2017; date of current version March 10, 2017. This letter was recommended for publication by Associate Editor C. Gosselin and Editor P. Rocco upon evaluation of the reviewers' comments. This work was supported in part by the National Science Foundation under Grant CNS-1320561.

F. Jiang and J. Zhao are with the Department of Mechanical Engineering, Colorado State University, Fort Collins, CO 80523 USA (e-mail: jiangfeicq@gmail.com; Jianguo.Zhao@colostate.edu).

Arun K. Kota is with the Department of Mechanical Engineering and the School of Biomedical Engineering, Colorado State University, Fort Collins, CO 80523 USA (e-mail: arun.kota@colostate.edu).

N. Xi is with the Department of Industrial and Manufacturing Systems Engineering, The University of Hong Kong, Hong Kong Special Administrative Region, China (e-mail: xining@hku.hk).

M. W. Mutka and L. Xiao are with the Department of Computer Science and Engineering, Michigan State University, East Lansing, MI 48824 USA (e-mail: mutka@cse.msu.edu; lxiao@cse.msu.edu).

Color versions of one or more of the figures in this letter are available online at http://ieeexplore.ieee.org.

Digital Object Identifier 10.1109/LRA.2017.2662738

using a spring based mechanism to generate a larger thrust for the robot to jump. They carefully designed the supporting legs and center of gravity to guarantee the continuous jumping ability of the robot.

Despite existing research on water jumping robots, two issues remain underexplored, which are critical in achieving better jumping performances. The first issue is how to optimally design a chosen jumping mechanism to minimize the robot's weight. Answering this question can improve the jumping performance as jumping highly depends on a robot's weight [2]. The second issue is how to predict the jumping performance by modeling the whole jumping process starting from the instant release of energy in a storage medium to the take-off from the water surface. Such a model can elucidate the whole jumping process comprised of multiple, complicated, and spatial-temporal phases involving different types of energy transfers, dynamic interactions between solids and liquids, and hydrodynamics. Further, such a model can be combined with the mechanism design to formulate an integrated optimization problem to maximize the jumping performance.

In this paper, we aim to address these two issues by presenting the design, modeling, and experimentation of a water jumping robot (the prototype is shown in Fig. 1). For the first issue, we optimize a jumping mechanism driven by a carbon fiber (CF) strip to minimize the torque that is required to charge energy into the strip, thereby minimizing the robot's weight with an optimal motor and appropriate supporting structures. For the second issue, we developed a general and simplified mathematical model to predict the jumping performance. This model can simulate the velocity profile of the robot during the whole jumping process using a momentum-impulse relationship, a predicted flapping impulse time, and a hydrodynamic model to capture the dynamic process before the robot leaps out of water. Such a model can also be leveraged to predict the performance for other water jumping robots.

The rest of this paper is organized as follows. First, we elaborate the robot's design, including mechanism designs and optimizations. Second, we describe a general mathematical model for jumping from water surface. Finally, we present simulation results using the mathematical model and conduct experiments on robot prototypes to compare with the proposed modeling methods.

II. Robot Design

The general design of the robot is illustrated in Fig. 2 with major components labeled. The robot is made of one hollow body connected to two flapping wings via rotational joints. A carbon fiber strip is connected to the two wings through another two rotational joints. A DC motor actuated intermittent gear train charges and releases energy in the carbon fiber strip. A cable connects the two wings to the output of the gear train, which is labeled as a rotation link in Fig. 2. When the motor rotates, it drives the intermittent gear train, and the rotation link rotates in clockwise direction, which forces the cable to move upward, resulting in the wings' inward rotation. In this way, the carbon fiber strip bends to store energy. When gear 2 rotates to a critical point where some of its teeth are removed, it is separated from gear 3, and the energy in the carbon fiber strip is instantly released to force the wings to rotate outward to flap the water, which in turn will make the robot jump from water surface.

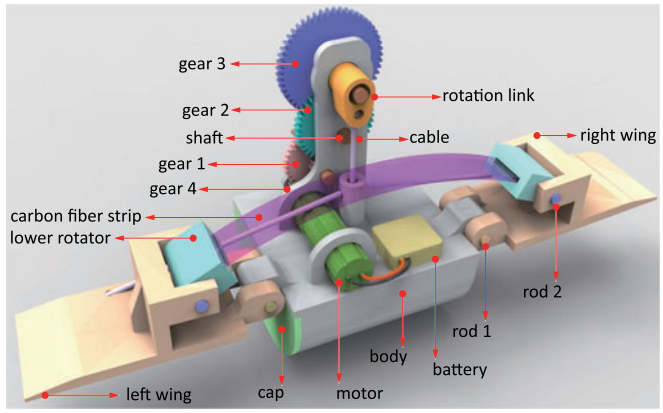

Fig. 2. Solid model for the water jumping robot.

According to functions, we divide the robot into two parts: jumping mechanism and energy mechanism. In this section, we present the design and analysis of each mechanism. Additionally, we also optimize the mechanisms to minimize the required torque for charging energy to the robot.

A. Jumping Mechanism

The jumping mechanism transforms the stored energy in the carbon fiber strip to the kinetic energy for take-off. For this mechanism, the two wings are symmetrically placed at two sides of the robot body. In order to select the appropriate DC motor and design the gear train unit, we need to calculate the force and torque required to charge energy into the carbon fiber strip.

Fig. 3 illustrates the mechanism at two positions: the initial position (black solid lines) corresponding to when the carbon fiber is straight, while the current position (red dashed lines) corresponding to when the rotation link rotates to an angle of λ. The point P represents the rotation link's free-end that connects to one end of the cable (see Fig. 3), and the other end of the cable is fixed symmetrically at point G and J. Point D is a fixed anchor location on the robot that the cable can go through. With the proposed jumping mechanism, the force F_2 rotates the two wings inward when actuated, which consequently bends the carbon fiber strip. In this way, the energy is charged into the strip. Once we remove the inward force (F_2) by actuating the intermittent gear train to the critical point, the stored energy is transformed to the robot's kinetic energy for take-off. This mechanism simplifies the design by directly using an elastic strip as the energy storage medium.

To get the required torque (T in Fig. 3) that should be provided by the gear train, we first obtain the horizontal force F_1 shown in Fig. 3 for bending the carbon fiber strip to an angle of α, and then use F_1 to derive the force F along the cable attached to the rotation link. We also obtain the moment arm for force F with

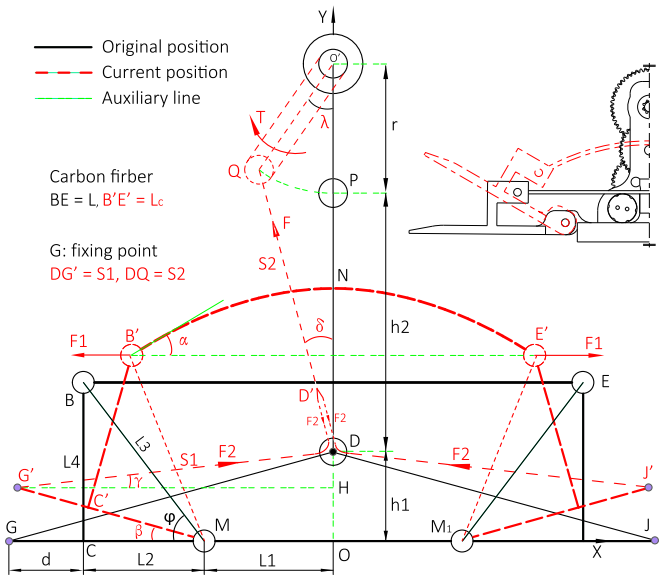

Fig. 3. Schematic for static force analysis: this figure illustrates two positions for the water jumping robot during the energy charge process. The figure in the upper-right corner illustrates these two positions using half of the solid model. Letters with a prime represent labels for the current position.

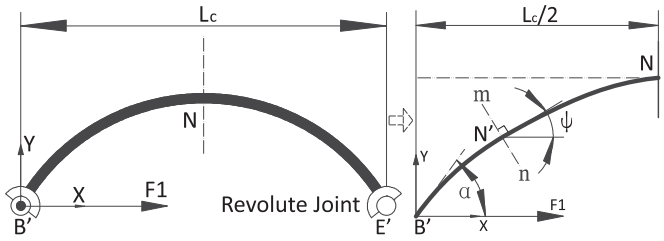

Fig. 4. Analysis of static forces for the carbon fiber strip. The mechanism is shown in the left figure, where an elastic strip connects the two wings to the main body via two revolute joints. The free body diagram for half of the strip (B'N) is shown in the right figure. Point N' is a random point selected on the strip, and line 'mn' is perpendicular to the tangent line at point N'.

respect to point O' by investigating the geometrical relationship shown in Fig. 3.

The principles for deflections of buckled slender bars should be employed to calculate how much force is required to bend the strip [21], [22] for a given bending angle of α. The statics for half of the strip is equivalent to the case shown on the right side of Fig. 4, where a slender bar is fixed to the ground at point N and has a free end at point B'. A horizontal inward force F_1 is applied at B'. We set up a coordinate system with origin at B' and the axes along the horizontal and vertical directions as shown in Fig. 4.

As for the bending behavior analysis of the strip, we take the cross section at point N' (represented by the line mn), then we obtain [22]

$$EI\frac{d^2\psi}{ds^2} = -F_1\sin(\psi), \tag{1}$$

where E is Young's modulus, I is area moment of inertia, s is the curve length from B' to N', and ψ is the angle between the tangent line of the bar at point N' and the horizontal line. Let $K = \sqrt{F_1/EI}$ and the total length of the strip be L, which will not change during the elastic deformation process.

For large deflection of buckled bars, K is calculated by [22]

$$K = \frac{1}{L}\int_0^{\frac{\pi}{2}} \frac{1}{\sqrt{1-p^2\sin^2(\Phi)}}\mathrm{d}\Phi, \tag{2}$$

where $p = \sin(\frac{\alpha}{2})$.

For a given α, the horizontal extension force F_1 is [22]

$$F_1 = K^2EI = \frac{EI}{L^2}\left(\int_0^{\frac{\pi}{2}} \frac{1}{\sqrt{1-p^2\sin^2(\Phi)}}\mathrm{d}\Phi\right)^2. \tag{3}$$

The projection length (line $B'E'$ in Fig. 3 and L_c in Fig. 4) of the strip with respect to the horizontal direction is derived as

$$L_c = \frac{1}{K}\int_0^{\frac{\pi}{2}} \left(\frac{1-2p^2\sin^2(\Phi)}{\sqrt{1-p^2\sin^2(\Phi)}}\right)\mathrm{d}\Phi. \tag{4}$$

To obtain the cable tension F_2 once F_1 is solved, we need to derive several angles labeled in Fig. 3 using geometric relationships. For example, the rotation angle for each wing $\beta = \angle G'MG$ can be derived as

$$\begin{aligned}\beta &= \angle B'MG - \angle BMG \\ &= \arccos\left(\frac{L_c/2 - L_1}{L_3}\right) - \arccos\left(\frac{L_2}{L_3}\right),\end{aligned} \tag{5}$$

where $L_1 = |OM|$, $L_2 = |MC|$, $L_3 = |BM|$. Note that some undefined parameters in texts can be found in Fig. 3. Similarly, angle $\lambda = \angle QO'P$, $\gamma = \angle DG'H$, $\varphi = \angle BMG$, and $\delta = \angle QDP$ can be calculated by geometrical relationships.

Since the moment from F_1 and F_2 acted on the wings with respect to point M should be equal, then F_2 can be expressed as

$$F_2 = \frac{L_3\sin(\beta+\varphi)}{(L_2+d)\sin(\beta+\gamma)}F_1. \tag{6}$$

Initially, DP, DG and DJ are three independent wires which are fixed together at point D. When we turn on the motor to bend the carbon fiber strip, point D moves to point D', and wire DD' is parallel to wire $D'Q$ (refer to Fig. 3). For a quasi-static state, point D' is balanced by the cable tensions in the 3 cables, then we can get $F = 2F_2$.

Finally, we calculate the torque required to charge energy to the carbon fiber strip

$$T = F(r+h_2)\sin\delta = \frac{2L_3\sin(\beta+\varphi)(r+h_2)\sin\delta}{(L_2+d)\sin(\beta+\gamma)}F_1. \tag{7}$$

B. Design Optimization

Using (7), we can obtain the torque profile T during the energy charge process by varying the value of α from zero to some angle with a small step size. In fact, the torque profile depends on the values of L_1, L_2, h_1, h_2, r and d since all the other angles and lengths can be derived from them. Note that we fix the value of $L_4 = 6.3$ mm to avoid interference with the battery. Consequently, L_3 should not be considered as a

parameter since $L_3 = \sqrt{L_2^2 + L_4^2}$. For each torque profile, a peak torque ($T_{\max}$) exists. With the same jumping mechanism and bending angle, a smaller peak torque can lead to a smaller mass and geometric size for the robot design. Therefore, it is necessary to minimize this peak torque by choosing the optimal geometric dimensions of the robot.

In the following, we perform the optimal design in four steps: 1) identify the optimization variables, 2) formulate the objective function, 3) obtain the constraints for geometric parameters, 4) solve the constrained problem with optimization algorithms.

1) The variables are L_1, L_2, h_1, h_2, r, and d since α will vary from 0 to some angle (we let this angle be $\pi/3$ due to practical constrains of the intermittent gear train).
2) Given L_1, L_2, h_1, h_2, r, and d, a torque profile exists as α running from 0 to $\pi/3$. The objective is to find the optimal L_1, L_2, h_1, h_2, r, and d such that the peak torque in the corresponding profile is minimum among all profiles. Then the objective function is the peak torque in the profile:

$$g(L_1, L_2, h_1, h_2, r, d) = \max_{\alpha \in [0, \pi/3]} T(L_1, L_2, h_1, h_2, r, d, \alpha) \tag{8}$$

3) The next step is to designate the range for all optimization variables depending on the mass distribution and geometric dimensions. With practical size and implementation considerations, we assign appropriate linear constraints for L_1, L_2, h_1, h_2, r, and d to formulate the optimization problem as

$$\begin{aligned} &\text{minimize} \quad g(L_1, L_2, h_1, h_2, r, d) \\ &\text{subject to}: 15.0 \le L_1 \le 17.5, \quad 8.0 \le L_2 \le 10.0, \\ &\qquad\qquad 7.5 \le h_1 \le 10.0, \quad 8.0 \le h_2 \le 13.0, \\ &\qquad\qquad 3.0 \le r \le 5.0, \quad 0 \le d \le 10.0, \end{aligned} \tag{9}$$

where the length unit (millimeter) is omitted.

4) Finally, we use optimization function *fmincon* in Matlab (2014b, The Mathworks Inc.) to optimize the design. The optimized dimensions are $L_1 = 17.5$ mm, $L_2 = 10.0$ mm, $h_1 = 10.0$ mm, $h_2 = 8.5$ mm, $r = 3.0$ mm and $d = 10$ mm. The length of the carbon fiber strip can be calculated as $L = 2(L_1 + L_2) = 55$ mm.

With the optimal dimensions, we calculate and plot the force (F) and torque (T) with respect to the strip bending angle (α) in Fig. 5. From the figure, it is obvious to observe that F decreases as α increases, while the torque (T) initially increases with α and reaches its peak value ($T_{\max} = 0.2176$ N.m) when $\alpha = 37.5^\circ$, then it keeps decreasing to zero when $\alpha = 58^\circ$. $T_{\max}$ is the global maximum of the torque.

C. Energy Mechanism

The energy mechanism can apply and remove the torque T in Fig. 3, the rotation link $O'Q$ is connected to the output of an intermittent gear train. The gear train unit is not displayed in Fig. 3, but it is shown in the solid model (Fig. 2) and also illustrated in detail in Fig. 6. A cable connects the rotation

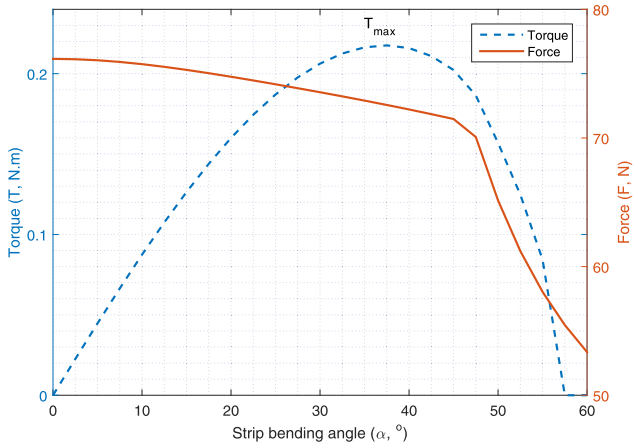

Fig. 5. Torque (required to charge energy into the carbon fiber, T in Fig. 3) and force (cable tension, F in Fig. 3) profiles with optimal dimensions.

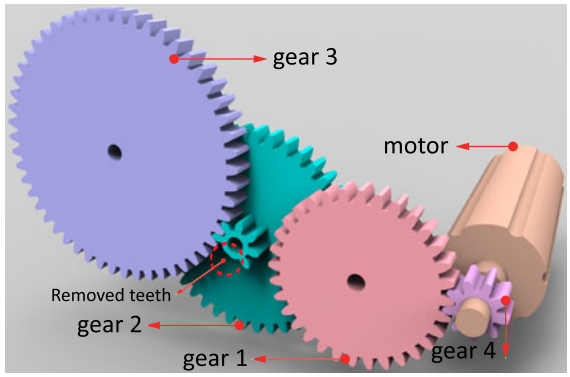

Fig. 6. Illustration of the intermittent gear train.

link to the two wings. Therefore, if the rotation link rotates in the clockwise direction, the cable pulls both wings inward. Once the rotation link passes the critical point, the energy will be released due to the intermittent gearing mechanism. We choose intermittent gear for actuation rather than other methods like one-way bearing [2], [3] because of the former's simplicity and smaller weight.

To design an appropriate gear train and select a corresponding DC motor to bend the carbon fiber strip, we refer back to Fig. 5. The global maximum torque ($T_{\max}$) of the robot is 0.2176 N.m, which should be smaller than the output torque from the gear train.

We select the most general form of intermittent gearing mechanism for our robot [23] as shown in Fig. 6. In order to guarantee a high coefficient of safety while balancing geometric dimensions, we chose a three-stage intermittent gear train unit with a total speed reduction ratio of 115.6, and it is made of four gears: a motor gear with 9 teeth, a compound gear with 32/8 teeth, an intermittent gear with 40/8 teeth, and a spur gear with 52 teeth. Gear 2 is an ordinary gear designed for continuous rotation but with two teeth being manually removed. This design allows gear 3 to rotate one-fourth of a turn for each turn of gear 2. When gear 2 and 3 are not meshed, force (F) and torque (T) are released under the tension (F_1) from the carbon fiber strip.

The miniature DC motor is selected (Part NO. GH6122S from Gizmoszone) with a nominal voltage of 3V and a mass of 1.7 grams. With a speed reduction ratio of 115.6 for the gear train and a stall torque of 2.45 mN.m of the motor, the maximum torque at the end of the gear train is 283.2 mN.m, which is around 1.3 times the maximum required torque $T_{\max}$ (217.6 mN.m) obtained from the torque profile in Fig. 5. With a safety coefficient of 1.3, this motor is strong enough even if the carbon fiber strip is bent to a larger deformation angle.

III. Hydrodynamic Analysis

We can predict the robot's jumping performance by establishing a mathematical model that captures the dynamic process right after the energy is released and right before the robot jumps out of water. This can be accomplished in the following steps. First, we calculate the stored energy in the carbon fiber strip by utilizing elastica theories, and then obtain the wings' angular velocity when they begin to flap the water. After that, a governing equation of the robot's velocity before jumping out of water can be derived by using theorem of impulse and hydrodynamic models. Finally, we obtain the jumping height by estimating the take-off velocity when the robot jumps out of the water.

To obtain the energy stored in the carbon fiber, we treat the strip as a circular arc (radius R_{cf}, $R_{cf} = L/(2\alpha)$) during the energy charging process. Then the energy stored in the carbon fiber is [24]

$$E_{\text{bend}} = \frac{EIL}{2R_{cf}^2} = \frac{2EI\alpha^2}{L}, \tag{10}$$

where the definitions of E, I, L, and α can be found in Section II-A.

Before the two wings flap the water, we assume the energy stored in the carbon fiber strip is fully transformed to the rotational kinetic energy of two wings

$$E_{\text{bend}} = 2\left(\frac{1}{2}I_w\omega^2\right) = I_w\omega^2, \tag{11}$$

where $I_w = 4.18 \times 10^2$ g $\cdot$ mm^2, calculated by Creo (PTC Inc., Needham, MA), is the mass moment of inertia with respect to the rotational axis of the two wings, ω is the wing's maximum angular speed before flapping the water surface. Then ω can be obtained as

$$\omega = \left(\frac{E_{\text{bend}}}{I_w}\right)^{1/2} = \left(\frac{2EI\alpha^2}{LI_w}\right)^{1/2}. \tag{12}$$

The length and width of the two wings are $L_w = 28.4$ mm and $b_w = 15$ mm, respectively. When the wings flap the water, the corresponding hydrodynamic pressure force (F_{dw}) is derived as $\rho A_w U_w^2/2$, where ρ is the density of water, A_w is the area, and U_w is the linear velocity. Since the linear velocity of the wings varies along the length, we need to integrate the force

$$F_{dw} = C_d\int_0^{L_w}\frac{1}{2}\rho\left(b_w\cdot dx\right)\cdot(\omega x)^2 = \frac{C_d\rho b_w L_w^3 EI\alpha^2}{3LI_w}, \tag{13}$$

where $C_d = 1.1$ is the drag coefficient depending on Reynolds number and dimensions [25].

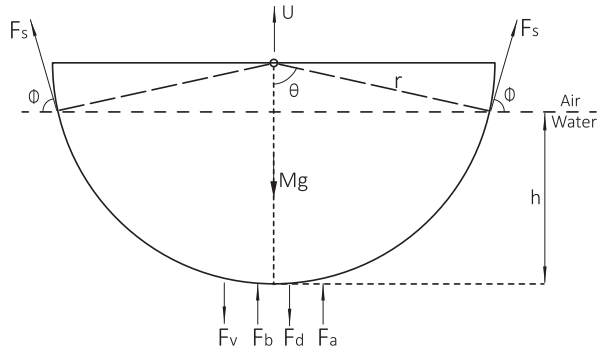

Fig. 7. Free-body diagram of the hollow body.

The angular velocity of the wings decreases to zero quite rapidly during the energy release process, and we roughly assume F_{dw} has a linear decreasing rate with respect to time. This force generates an impulse on the robot for a very short period of time (t_w), which will be mathematically predicted later. Depending on theorem of impulse, the robot gains a velocity of U_0 resulting from the impulse

$$U_0 = \frac{\bar{F}_{dw}\cdot t_w}{M} = \frac{\rho b_w L_w^3 EI\alpha^2 t_w}{6MLI_w}, \tag{14}$$

where $\bar{F}_{dw} = F_{dw}/2$ is the average of F_{dw}, and M is the total mass of the robot.

It's in general difficult to predict the impulse time (t_w) as the flapping is a complicated hydrodynamic process. Therefore, we simplify this process for the prediction. The average momentum of the wing during the flapping process is $\bar{P} = m\omega L_w/2$ (where m is the mass of the wing) after integration. Then the predicted impulse time t_p can be expressed as

$$t_p = \frac{\bar{P}}{\bar{F}_{dw}} = \frac{3\sqrt{2}m}{C_d\rho b_w L_w^2\alpha}\sqrt{\frac{LI_w}{EI}}. \tag{15}$$

The detailed calculation and validation of t_p will be discussed in Section IV-B.

After the robot gains an initial velocity of U_0, there are mainly six forces (see Fig. 7) exerting on the robot [26]: robot's gravity (Mg), surface tension (F_s), hydrostatic pressure force (F_b, buoyancy), hydrodynamic pressure force (F_d, form drag), viscous force (F_v) and added mass inertia force (F_a). In our case, since the Reynolds number $Re \gg 1$ in the jumping process, the viscous force ($F_v = \mu UA$, $\mu = 8.90 \times 10^{-4} Pa\cdot s$ @ 25 °C) is negligible compared with the hydrodynamic pressure force (F_d) [19]. The added mass force defines the force that fluid be accelerated around an accelerating body [27]. We don't count F_a into our model since we will only simulate the jumping process from the lowest point rather than the flapping phase. Therefore, the total force (F_{tot}) exerted on the robot is expressed as

$$F_{\text{tot}} = F_d + F_b + F_s\sin\phi, \tag{16}$$

where ϕ is the angle of the air-water interface at the three-phase contact line. For simplification, we assume $\sin\phi \simeq 1$ which means the surface tension force is in the vertical direction.

Suppose the robot leaves the water surface at a speed of U, then F_d, F_b, and F_s are calculated as [19]

$$F_d = \frac{1}{2}C_d\rho AU^2 = C_d\rho L_b U^2\sqrt{2Rh-h^2}, \tag{17}$$

$$F_b = \rho gV = \rho gL_b\left(\theta R^2 - (R-h)\sqrt{2Rh-h^2}\right), \tag{18}$$

$$F_s = \sigma L_p = 2\sigma\left(L_b + 2\sqrt{2Rh-h^2}\right), \tag{19}$$

where A is the reference area, L_b is the length of the body, R is the radius of the hollow body, $h \in [0, R]$ is the sinking depth from the body's bottom to the water surface, V is the volume immersed in the water, $g = 9.81\,\mathrm{m/s^2}$ is the gravitational constant, θ is the half central angle of the semi-cylindrical body, $\sigma = 72\,\mathrm{mNm^{-1}}$ is the surface tension coefficient of water, L_p is the body's perimeter at the air-water interface (see Fig. 7).

With the three forces, we can use Newton's second law during the robot's ascending process in water,

$$F_b + F_s - F_d - Mg - Ma = 0. \tag{20}$$

Since $a = \ddot{h}$, $U = \dot{h}$ and $\theta = a\cos(\frac{r-h}{r})$, then Eq. (20) is modified as

$$\frac{\partial^2 h}{\partial t^2} + \frac{C_d\rho L_b\sqrt{2Rh-h^2}}{M}\frac{\partial h}{dt} + \frac{\rho gL_b(R-h)+4\sigma}{M}\sqrt{2Rh-h^2} + \frac{Mg + 2\sigma L_b - \rho g\theta L_b R^2}{M} = 0. \tag{21}$$

Equation (21) is a partial differential equation of h with respect to time, and we can use numerical method to solve it as will be discussed in Section IV-B. Once h is solved, the velocity $U = \dot{h}$ can also be obtained. Finally, the take-off velocity from water surface can be derived to predict the jumping height.

IV. Simulation and Experimental Results

With the robot design and optimizations discussed in Section II, we build robot prototypes as shown in Fig. 1. In this section, we elaborate the prototype fabrication, present simulation results using the developed mathematical model, and discuss experimental results with the robot prototype.

A. Prototype Fabrication

The prototype fabrication for the robot includes customized parts and off-the-shelf components. Most of the designed components are fabricated by 3D printing (PolyJet, The Stratasys Inc.) with the VeroWhitePlus plus material. Rotational joints in the robot are realized by a simple pin-hole structure with the pins being cut from carbon fiber rods. All the four gears have a module of 0.3, and the part numbers for them are G309-97 from Didel SA, GC0.3-8/32-10, GC0.3-8/40-10, GC0.3-8/52-10 from Gizmoszone, respectively. The three gear shafts (from MicronWings) are made of stainless steel with brass keeper, and they have a diameter of 0.97 mm, a length of 23 mm, and a mass of 0.18 grams. The carbon fiber strip (T732Lm from The Composites Store, Inc.) has a rectangular cross-section with width of 6 mm and thickness of 0.8 mm and a Young's Modulus $E = 150$ Gpa. The actuation cable is a weather- and wear-resistant twine with a diameter of 0.84 mm. We selected an ultra low weight lithium ion battery (GM300815 from PowerStrain Inc.), which has a size of $3 \times 8 \times 15$ mm and a mass of 0.5 grams. The total mass of the robot is around 12.5 grams with all components assembled.

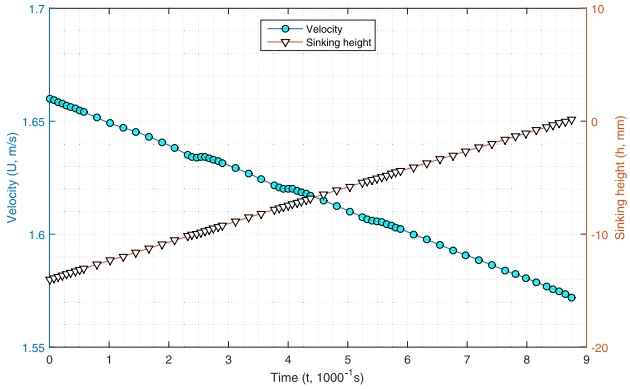

Fig. 8. Simulated robot's velocity profile with respect to time before jumping out of water using the numerical method.

B. Model Simulation

This subsection illustrates the simulation results to predict the jumping performance using the mathematical model in Section III.

As for the initial validation, we select a less stronger carbon fiber strip with a cross-section dimension of 2.5 mm $\times$ 0.6 mm since the pre-selected strip generates larger force and can fail the robotic mechanism. In order to store enough energy for take-off, we pre-load the elastic strip with a bending angle of $\pi/8$, then the total bending angle α can reach $\pi/4$ before the release of energy owing to the extra bending resulted from the intermittent gear train. With such a setup, the predicted impulse time t_p is calculated as 0.0015 s from Eq. (15). By analyzing the recorded video of the jumping process using a high speed camera (details for the experiment will be discussed in the next subsection), we can also estimate the impulse time. The starting point is defined when the wings start to flap the water, while the end point means the wings stop rotating around the axles. The impulse time is estimated as $t_w \approx 0.002$ s by checking the video frame by frame. The 25% difference between t_p and t_w is mainly resulted from the frame rate limitation of the high speed camera. The resolution is reduced and cannot capture the whole jumping process with a higher frame rate. With $t_w \approx 0.002$ s, the initial velocity of the robot U_0 is calculated as 1.66 m/s from (14).

We numerically solve the partial differential equation (21) and plot the velocity profile of the robot with respect to time as shown in Fig. 8. The ODE solver 'ODE45' in Matlab (2014b, The Mathworks Inc.) is used to obtain the solution. The boundary condition is the initial jumping velocity (U_0) and sinking height (h_0) of the hollow body. Fig. 8 shows that the sinking height increases from a negative value of h_0 to zero, but the robot's velocity decreases from $U_0 = 1.66\,\mathrm{m/s}$ because of the form drag and gravity.

From the velocity profile, we estimate the vertical velocity when the robot just gets out of water to be $U_r \approx 1.57\,\mathrm{m/s}$. The

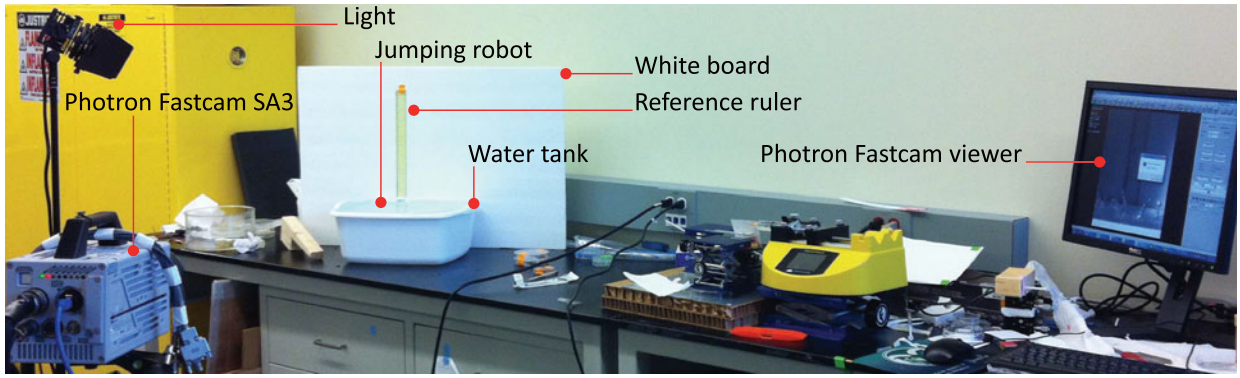

Fig. 9. Jumping test set-up.

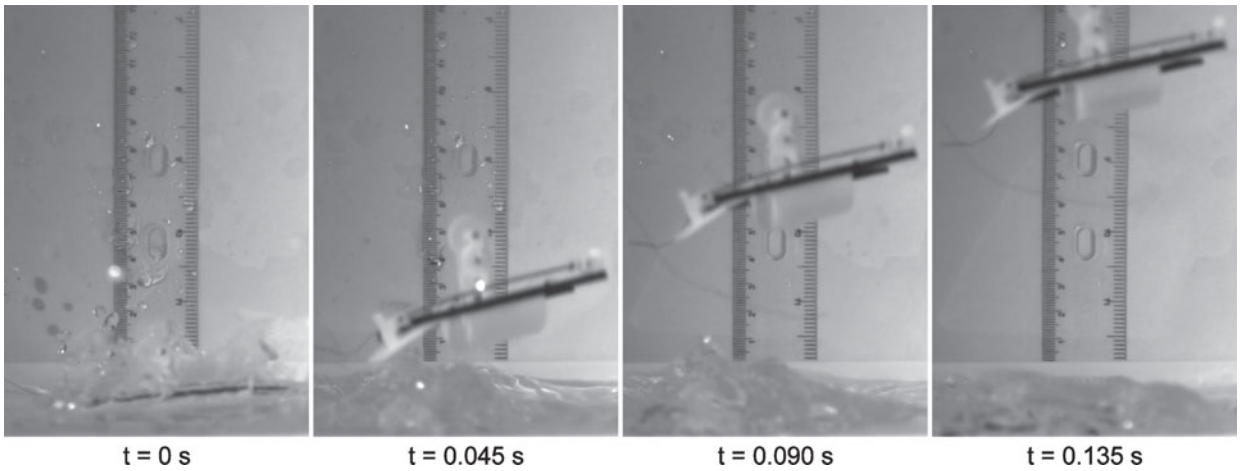

Fig. 10. Images from the video recorded by a high speed camera were used to determine the robot's jumping performance—9 cm as shown in the last picture.

change in velocity between the end of the impulse (U_0) and take-off from the water surface (U_r) is only 5.4%. However, the drag force is large and water adhesion isn't negligible if the robot surface is not coated with hydrophobic materials, and the deceleration effect can be much larger (up to 30%). In addition, the effects vary for different sizes, shapes, and material properties.

With the take-off velocity $U_r = 1.57\,\mathrm{m/s}$, the jumping height (H_{tot}) above water surface can be calculated as

$$H_{\mathrm{tot}} = \frac{U_r^2}{2g} = 0.126\,\mathrm{m}. \tag{22}$$

C. Jumping Experiments

In this subsection, we discuss the experimental setups (see Fig. 9) and analyze the corresponding test results (see Fig. 10). Before conducting the jumping test, the body and two wings are coated with super hydrophobic materials named Ultra-Ever Dry (Ultratech International Inc.). The coating is critical in achieving a better jumping performance by reducing water adhesion. The robot gets wet easily if not coated, which can lead to a 20$\sim$ 40% shorter jumping height. In some cases, the robot cannot jump out of the water because of the disturbance and water adhesion.

After coating, we conduct experiments to test the robot's jumping capabilities. Since the battery gets wet easily and cannot work when the robot falls, as for initial test, we don't put the battery on the top surface of the hollow body. Instead, the DC motor is driven by the battery through two thin copper wires. The setups for jumping tests are shown in Fig. 9. We place the robot in a water tank in front of a reference ruler attached to a white board, then put the high speed camera (Photron Fastcam SA3) and light in appropriate positions. We also adjust the camera lens manually for an optimal quality. The position and view angle of the camera are also tuned to ensure the measurement accuracy. Finally, we record the jumping motion of the robot using a frame rate of 1000 fps and a resolution of 768 $\times$ 1024.

After recording the video, images from the video are analyzed to estimate the robot's jumping height by comparing the robot's vertical position with the reference ruler. The jumping height is defined between the water surface and the lowest point of the robot at the peak. As see from Fig. 10, the robot can jump up to 9.5 cm, and it obtained an average jumping height of 9 cm with standard deviation of 0.32 cm in five successful trials. The discrepancy between the theoretical jumping height of 12.6 cm and the true height of 9 cm may come from the inaccurate estimation of t_w, the neglected frictions in robot's revolute joints, and the slight pull from the copper wires.

Compared with the water jumping robots described in the introduction (see Table I), our robot has a good overall performance although it has the largest weight. Further, our robot is large enough to carry sensors and subsystems for aquatic mobile sensing when compared to the robot in [17] and the robotic

TABLE I
COMPARISON WITH EXISTING ROBOTS WITH THE WATER JUMPING ABILITY

Robot Name	Robotic mechanism/Actuation	Size (L × W × H, mm)	Mass (gram)	Max height (mm)
Water jumping robot [17]	Latch driven shape memory alloy	L26 × W13	0.510	26
Robotic insects [18]	(NiTi) SMA actuator	L20	0.068	142
Water-Jumping Microrobot [19], [20]	DC motor and reduction gear unit	L250 × W150	10.2∼11.0	120∼140
CF driven Water jumping robot	**DC motor, CF strip and intermittent gear train unit**	**L100 × W28**	**12.5**	**95**

insect [18]. In addition, it is smaller than the microrobot [19], [20] with a similar mass.

To further improve the performance of the proposed robot and more generally on any water jumping robot, we believe that an integrated optimization considering the major dimensions and components together with the dynamics during the whole jumping process can lead to better performances. In fact, similar methods have been recently proposed for ground jumping robot [28]. However, since the water jumping process is much more complicated than ground jumping, we will leave such an integrated optimization as future work.

V. CONCLUSION

In this paper, we describe the development of a new miniature robot that can jump from water surface. The design of the robot includes a carbon fiber strip to store the energy, an intermittent gear train driven by a miniature DC motor, and a symmetric wing system to flap the water. The final robot has a compact size ($100 \times 28 \times 50$ mm) and a small mass (12.5 grams). We also develop a mathematical model that captures the dynamic process before the robot jumps out of water to predict the jumping performance. Experimental results show that the robot can achieve an average jumping height of 9 cm, which is less than the height predicted by the mathematical model. The errors may result from several simplifications in the model. The robot is an ideal platform for mobile sensing in aquatic environments if equipped with the self-recovery ability. Future work will try to improve the jumping performance using an integrated optimization framework considering both the mechanism design and the dynamics during the jumping process.

ACKNOWLEDGMENT

The authors thank Dr. W. Wang for showing us how to use the high-speed camera for the jumping test and the anonymous reviewers for their helpful and constructive suggestions for this paper.

REFERENCES

[1] F. J. Cintron, K. Pongaliur, M. W. Mutka, L. Xiao, J. Zhao, and N. Xi, "Leveraging height in a jumping sensor network to extend network coverage," *IEEE Trans. Wireless Commun.*, vol. 11, no. 5, pp. 1840–1849, May 2012.

[2] J. Zhao *et al.*, "MSU jumper: A single-motor-actuated miniature steerable jumping robot," *IEEE Trans. Robot.*, vol. 29, no. 3, pp. 602–614, Jun. 2013.

[3] J. Zhao, W. Yan, N. Xi, M. W. Mutka, and L. Xiao, "A miniature 25 grams running and jumping robot," in *Proc. IEEE Int. Conf. Robot. Autom.*, 2014, pp. 5115–5120.

[4] M. Kovac, M. Fuchs, A. Guignard, J.-C. Zufferey, and D. Floreano, "A miniature 7g jumping robot," in *Proc. IEEE Int. Conf. Robot. Autom.*, 2008, pp. 373–378.

[5] M. Kovač, M. Schlegel, J.-C. Zufferey, and D. Floreano, "Steerable miniature jumping robot," *Auton. Robots*, vol. 28, no. 3, pp. 295–306, 2010.

[6] J. Zhang, G. Song, Y. Li, G. Qiao, A. Song, and A. Wang, "A bio-inspired jumping robot: Modeling, simulation, design, and experimental results," *Mechatronics*, vol. 23, no. 8, pp. 1123–1140, 2013.

[7] M. A. Woodward and M. Sitti, "Multimo-bat: A biologically inspired integrated jumping–gliding robot," *Int. J. Robot. Res.*, vol. 33, no. 12, pp. 1511–1529, 2014.

[8] A. P. Gerratt and S. Bergbreiter, "Incorporating compliant elastomers for jumping locomotion in microrobots," *Smart Mater. Structures*, vol. 22, no. 1, 2012, Art. no. 014010.

[9] N. W. Bartlett *et al.*, "A 3D-printed, functionally graded soft robot powered by combustion," *Science*, vol. 349, no. 6244, pp. 161–165, 2015.

[10] A. L. Desbiens, M. Pope, F. Berg, Z. E. Teoh, J. Lee, and M. Cutkosky, "Efficient jumpgliding: Theory and design considerations," in *Proc. IEEE Int. Conf. Robot. Autom.,*, IEEE, 2013, pp. 4451–4458.

[11] G. Zeglin, "The bow leg hopping robot," Ph.D. dissertation, Robot. Inst., Carnegie Mellon Univ. Pittsburgh, PA, USA, 1999.

[12] G. Taylor, M. S. Triantafyllou, and C. Tropea, *Animal Locomotion*. New York, NY, USA: Springer Science & Business Media, 2010.

[13] X. Gao and L. Jiang, "Biophysics: water-repellent legs of water striders," *Nature*, vol. 432, no. 7013, pp. 36–36, 2004.

[14] D. L. Hu, B. Chan, and J. W. Bush, "The hydrodynamics of water strider locomotion," *Nature*, vol. 424, no. 6949, pp. 663–666, 2003.

[15] S. Sudo, M. Shiono, T. Kainuma, A. Shirai, and T. Hayase, "The kinematics of jumping of globular springtail," *J. Aero Aqua Bio-Mechanisms*, vol. 3, no. 1, pp. 85–91, 2013.

[16] S. P. Hopkin, *Biology of the Springtails:(Insecta: Collembola)*. Oxford, U.K.: Oxford Univ. Press, 1997.

[17] B. Shin, H.-Y. Kim, and K.-J. Cho, "Towards a biologically inspired small-scale water jumping robot," in *Proc. IEEE Int. Conf. Biomed. Robot. Biomechatronics*, 2008, pp. 127–131.

[18] J.-S. Koh *et al.*, "Jumping on water: Surface tension–dominated jumping of water striders and robotic insects," *Science*, vol. 349, no. 6247, pp. 517–521, 2015.

[19] J. Zhao, X. Zhang, N. Chen, and Q. Pan, "Why superhydrophobicity is crucial for a water-jumping microrobot? Experimental and theoretical investigations," *ACS Appl. Mater. Interfaces*, vol. 4, no. 7, pp. 3706–3711, 2012.

[20] J. Yan, K. Yang, T. Wang, X. Zhang, and J. Zhao, "A continuous jumping robot on water mimicking water striders," in *Proc. IEEE Int. Conf. Robot. Autom.*, 2016, pp. 4686–4691.

[21] R. M. Jones, *Buckling of Bars, Plates, and Shells*. Blacksburg, VA, USA: Bull Ridge Corporation, 2006.

[22] S. P. Timoshenko and J. M. Gere, *Theory of Elastic Stability*. North Chelmsford, MA, USA: Courier Corporation, 2009.

[23] F. Jones, *Ingenious Mechanisms Vol I*. New York, NY, USA: Industrial Press, 1930.

[24] T. A. Waigh, *The Physics of Living Processes: A Mesoscopic Approach*. Hoboken, NJ, USA: Wiley, 2014.

[25] M. Sadraey, *Aircraft Performance: Analysis*. Saarbrücken, Germany: VDM Publishing, 2009.

[26] J. W. Bush and D. L. Hu, "Walking on water: Biolocomotion at the interface," *Annu. Rev. Fluid Mech.*, vol. 38, pp. 339–369, 2006.

[27] J. Glasheen *et al.*, "A hydrodynamic model of locomotion in the basilisk lizard," *Nature*, vol. 380, no. 6572, pp. 340–341, 1996.

[28] V. Zaitsev, O. Gvirsman, U. B. Hanan, A. Weiss, A. Ayali, and G. Kosa, "A locust-inspired miniature jumping robot," *Bioinspiration Biomimetics*, vol. 10, no. 6, 2015, Art. no. 066012.